

# ON THE INTERACTION OF STREAMWISE VORTICITY WITH A ROTATING TURBINE BLADE

*C. M. Schneider – D. Schrack – M. G. Rose – S. Staudacher*

Institute of Aircraft Propulsion Systems, Pfaffenwaldring 6, 70569 Stuttgart, Germany,  
[carsten.schneider@ila.uni-stuttgart.de](mailto:carsten.schneider@ila.uni-stuttgart.de)

*Y. Guendogdu – K. Engel*

MTU Aero Engines GmbH, Dachauer Straße 665, 80995 Munich, Germany

## ABSTRACT

This paper addresses the unsteady formation of secondary flow structures inside a rotor passage. The first stage of a two-stage low pressure turbine is investigated at a Reynolds Number of 75000. The configuration represents the third and the fourth stages of an engine low pressure turbine. The vane-rotor interactions at hub are discussed in the relative frame of reference using the streamwise vorticity to identify the flow structures and interaction processes involved. A multi-stage URANS prediction which is validated by time-averaged five-hole probe data at inlet and exit of the rotor provides the time-resolved data set required. An interaction mechanism is revealed which is responsible for the creation of rotating structures which are fixed in space in the absolute frame of reference at rotor exit. The wakes and secondary flow structures of the nozzle guide vane transform the secondary flow structures at the rotor hub unsteadily. The time-averaged isentropic efficiency distribution at rotor exit is observed to be dominated by flow structures associated with the nozzle guide vane.

## NOMENCLATURE

### Abbreviations

CV	counter vortex
H	channel height [%]
NGV	nozzle guide vane
PV	passage vortex
rPV	rotor passage vortex
S	pitch [-]
t	time [s]
T	blade passing period [s]
TSSL	trailing shed shear layer

### Greek symbols

$\alpha$	circumferential angle [°]
$\eta$	efficiency [-]

### Vector quantities

$\vec{e}$	normalized unit vector [-]
$\vec{\omega}$	vorticity vector [-]

### Subscripts

0	stagnation quantity
ex	rotor exit
in	turbine inlet
is	isentropic quantity
low	lower (TSSL)
s, n, r	streamwise, normal, and radial
up	upper (TSSL)

## INTRODUCTION

The flow in turbines which doesn't follow the primary direction is called secondary flow whereat the primary flow direction is defined by the design turning of each blade row. According to Langston (2001) secondary flows are produced by viscous effects and endwalls and thus, every turbine is affected. Secondary flows mix out, produce losses and diminish the work output of a turbine. They can be responsible for 30 % to 50 % of the aerodynamic losses in turbines; see Sharma and Butler (1987). Academia and industry have performed many studies to explain the

basic patterns, the sources, and influence parameters of secondary flows during the last decades. These studies are performed on linear (planar) cascades mostly and come up with a basic picture of secondary flows as presented e.g. by Sieverding (1985) or Sharma and Butler (1987). Fig. 1 gives an overview about the main secondary flow structures involved. It shows the evolution of the horse shoe vortex and the passage vortex. The former develops in front of the leading edge as a result of the endwall boundary layer approaching the stagnation point and the latter forms due to the turning of the endwall boundary layer inside the passage.

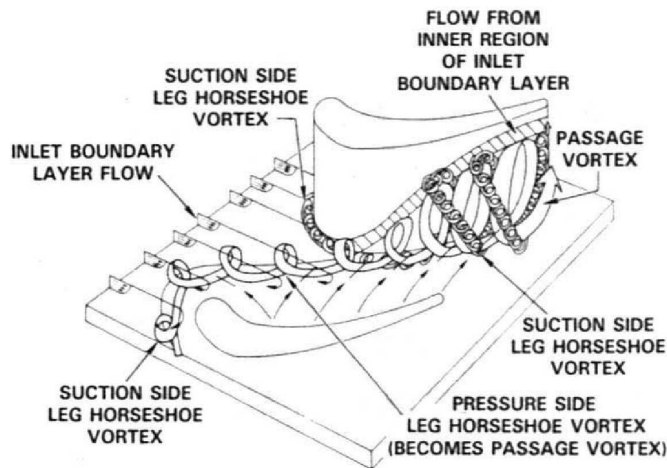


**Fig. 1 Cascade endwall flow structure reported by Sharma and Butler (1987)**

A number of important parameters are neglected when secondary flow is studied in linear cascades. These are annular geometry, radial migration, rotation of the frame of reference, leakage flows entering the main flow unsteadily, and vane-rotor interactions. Therefore the three-dimensional secondary flow patterns of real turbines are more complex and less understood. Further understanding of unsteady vane-rotor interactions has the potential to improve turbine design. Vortex-blade interaction phenomena in a low aspect-ratio turbine rig have been investigated by Binder et al. (1985, 1987, and 1989). Similar studies have been performed by Aurahs et al. (2009) in a water flow model turbine. Both authors have surveyed vortex break down phenomena experimentally inside a rotor passage in terms of turbulence production and convection. Furthermore Pullan (2006) reports about vane-rotor interaction phenomena of a low-speed turbine stage. He proposes a formation mechanism inside the rotor passage which transforms flow structures related to the nozzle guide vane (NGV) into vortices at rotor exit. The present paper addresses the interaction of wake and secondary flow structures of the nozzle guide vane with a rotating turbine blade inside an engine representative low pressure turbine to shed light onto this complex three-dimensional process.

## EXPERIMENTAL SETUP

The experimental data shown in this paper has been measured in the Advanced-Turbine-Research-Demonstrator-Rig. The ATRD-Rig is an engine representative two-stage low pressure axial turbine designed by MTU Aero Engines GmbH and tested at the Institute of Aircraft Propulsion Systems at Stuttgart University. It operates in an altitude test facility at Reynolds numbers from 180000 down to 35000. The rig Mach and the Reynolds number are preserved to match the engine. This setup simulates a low pressure turbine operated at high altitudes. The turbine is designed with a conventional blade loading slightly above two and has typical aspect ratios around 2.5. On average, the Mach numbers at each vane exit are approximately 0.6. The configuration represents the third and the fourth stages of an engine low pressure turbine. The blade numbers are 60:55:58:57. Schinko (2012) provides a detailed description of the ATRD-Rig characteristics. A schematic of the rig is given in Fig. 2. The planes which are relevant for the analysis presented are labelled in the schematic.

Five-hole probe traverses have been performed within each axial gap of the research turbine. The pneumatic probe used is shown in Fig. 3 in front of a NGV segment. The conical probe head diameter is 3mm. Right above the probe head a thermo couple is incorporated into the probe shaft to be able to measure temperatures. The radial difference between the location of the temperature and the pressure measurements is corrected in the data reduction process. The assumption of laminar flow around the thermo couple has been made to correct for the recovery process. Following Nitsche and Brunn (2006) a constant recovery factor of 0.85 has been chosen to calculate the stagnation temperature. The absolute uncertainties of the five-hole measurement are  $\pm 4\%$  of the dynamic head for the stagnation pressure,  $\pm 1\text{K}$  for the stagnation temperature, and  $\pm 1.6^\circ$  for the circumferential angle. The uncertainty analysis includes uncertainties due to probe positioning as well as due to the calibration process. Please note that the absolute pressure level in the turbine is lower than approximately 0.2 bar. Generally the traverse area covers 1.1 pitches in the circumferential direction and approximately 100 % span. The five-hole probe traverse at NGV exit has a resolution of 30 points in the radial as well as in the circumferential direction. It extends from 0.8 % to 96.0 % span. The traverse plane at NGV exit is located at 50 % axial gap between the NGV trailing edge and the rotor leading edge. At rotor exit the five-hole probe traverse has a resolution of 18 points in the circumferential and 30 points in the radial direction. The span from 2.0 % to 98.0 % is covered by the measurement. The traverse plane is located at 66 % gap between the rotor trailing edge and the leading edge of the downstream NGV. The radial spacing is not equidistant. It is reduced in the hub and tip regions to improve the resolution of the secondary flow areas; see Kuerner et al. (2010).

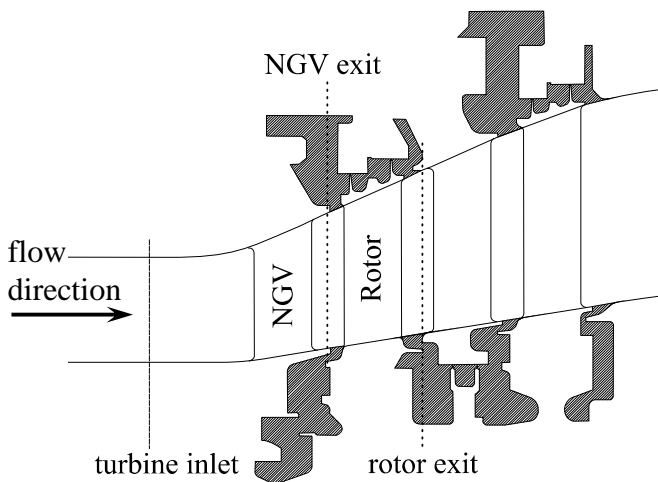


**Fig. 2 Schematic of the ATRD-Rig; traverse planes as dotted lines**

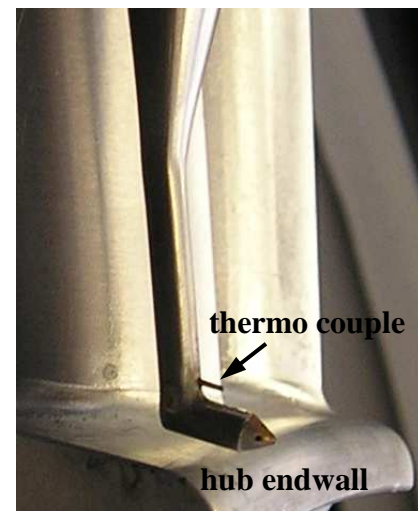


**Fig. 3 Five-hole probe with thermo couple in front of a vane segment**

## ANALYSIS METHODOLOGY

The vorticity vector  $\vec{\omega}$  in the cylindrical coordinate system of the rig is derived from the five-hole probe data. It is calculated using a compressible approach invented by Niehuis et al. (1990). To study the secondary flow components it is appropriate to evaluate the vorticity in a new coordinate system which is aligned with the streamwise direction. The streamwise direction (s) is defined by the local direction of the velocity whilst the normal (n) and the binormal directions are both perpendicular to this direction. The binormal direction is referred as the radial (r) direction in this paper there being negligible difference. That results in a set of three linearly independent vectors  $\vec{e}_s$ ,  $\vec{e}_n$ , and  $\vec{e}_r$ . The three components of vorticity are calculated using the scalar product according to eq. (1) below. Finally the vorticity components are non-dimensionalized using the NGV chord length and the mass-averaged velocity in the exit plane of

the row investigated. In the paper the vorticity derived from measurement data is referred to as measured vorticity.

The isentropic efficiency  $\eta_{is}$  presented in the paper is based on the control volume from turbine inlet to rotor exit shown in Fig. 2. It is defined in eq. (2). The indices “in” and “ex” refer to the turbine inlet and the rotor exit. The stagnation enthalpies are evaluated using a fluid model including humidity corrections as reported by Schinko (2012). The stagnation pressures and temperatures needed at inlet are measured via circumferentially distributed radial rakes whilst at rotor exit the five-hole probe is used. The measurements are recorded simultaneously to prevent influences due to working point fluctuations. Following this approach the local isentropic efficiency values are evaluated at rotor exit.

$$\omega_i = \vec{\omega} \cdot \vec{e}_i \quad \text{with } i = s, n, r \quad (1)$$

$$\eta_{is} = \frac{h_{0,in} - h_{0,ex}}{h_{0,in} - h_{0,ex,is}} \quad (2)$$

## NUMERICAL SETUP

The CFD predictions shown in the paper are the result of a multi-stage URANS simulation using TRACE (Turbomachinery Research Aerodynamics Computational Environment). It is a 3D compressible Navier-Stokes solver developed at the German Aerospace Center DLR in cooperation with MTU Aero Engines GmbH. A  $k-\omega$  two equation model is used for turbulence modelling; see Roeber et al. (2006). Transition is allowed on the suction sides whilst the pressure sides and endwalls are calculated with turbulent boundary layers. One pitch of the turbine geometry including the cavities has been sampled with a structured grid of approximately 7.5Mio cells. The simulated geometry includes fillet radii. The low Reynolds approach is applied on all but the cavity surfaces. Accordingly the  $Y^+ \approx 1$  criterion has been maintained on all surfaces approximately. The cavities are indicated in Fig. 2 by areas which are shaded. Wall functions are applied within the cavities. The setup with cavities leads to an improved secondary flow representation reported by Kuerner et al. (2011). For the unsteady simulation the blade number ratio is set to 1:1:1:1 via scaling the geometry. The blade loading is preserved during the scaling process. The relative change in blade count is in the range of 3 to 5 %. The influence of scaling is regarded as marginal due to the small changes in blade numbers; e.g. the predicted turbine efficiency changes by less than 0.03 %. Therefore it is neglected in the present analysis. One rotor blade passing ( $t/T=1.0$ ) is resolved with 96 time steps. Experimental results are applied as boundary conditions in the CFD prediction. The static pressures at hub and tip of the exit plane in the CFD are fitted to maintain the measured specific work of the turbine. The Reynolds number of the working point simulated is approximately 75000. It is based on the exit flow of the first nozzle guide vane.

## RESULTS

### Wake and Secondary Flow Structures of the Nozzle Guide Vane

In order to understand the nature of three-dimensional vane-rotor interactions, first the NGV exit flow field must be analyzed to identify the wake and secondary flow structures present. CFD results are used to give insight into the interaction phenomena inside the rotor. A comparison of experimental and time-averaged CFD data serves to validate the prediction. Generally, if not specifically mentioned the results are time-averaged and shown in the absolute frame of reference. The circumferentially mass-averaged distributions of the circumferential flow angle  $\alpha$  are presented in Fig. 4. The absolute uncertainty of the measurement is indicated by an error bar at approximately 25 % channel height. The main gradients are captured well by the CFD prediction. The predicted absolute value of the circumferential flow angle  $\alpha$  differs by approximately  $5^\circ$  from the measured

data in the hub region up to 15 % channel height. The larger overturning of the CFD prediction at the hub endwall indicates that the predicted intensity of the hub passage vortex is slightly overestimated. Fig. 5 shows contour lines of the measured radial vorticity  $\omega_r$  from the endwall up to 50 % channel height at NGV exit. The view is upstream. The measurement plane is located at 50 % axial gap between the NGV trailing edge and the rotor leading edge. The area of one pitch is marked by the grid overlaid on the contours. The pressure and the suction side regions within the wake can be identified by their rotational character. The vorticity highlights regions of rotating flow. These include shear layers as well as classical vortices. The region of negative radial vorticity is associated with the suction side whilst the region of positive radial vorticity with the pressure side part of the wake. The wake center and the free stream region have radial vorticity values around zero. By this means, the location of the wake center can be estimated. It is indicated with a dashed line at about -0.5 dimensionless pitch.

Having identified the location and the characteristics of the NGV wake in terms of vorticity the focus will now be on the secondary flow field at the hub. The classical secondary flow structures as presented in Fig. 1 can be identified using the streamwise vorticity  $\omega_s$ . The measured and the predicted streamwise vorticity are shown in Fig. 6 (a) and (b) using contour lines. The region of dashed lines on the suction side above the hub endwall can be clearly associated with the passage vortex. It rotates clockwise and transports endwall boundary layer fluid to and up the suction side. The position of the passage vortex, right above the endwall and close to the suction side of the wake, results from the radial and cross-passage pressure gradients. Generally, fluid of low momentum shows the tendency to migrate to regions of low static pressure. The counter clockwise rotating region which is indicated by the solid lines within the wake is associated with the shed vorticity of the NGV. According to Hawthorne (1955) it contains the trailing filament circulation and the trailing shed circulation. The two forms of circulation are only theoretically distinguishable from each other. Furthermore the region of trailing shed vorticity is presumably better characterized as a shear layer of suction and pressure side fluid with contrary signs of radial velocity components. Therefore, in this paper the region of positive vorticity within the wake is called trailing shed shear layer (TSSL) generally. Two distinct structures can be identified within the measured trailing shed shear layer. Both structures are marked with circular arrows in Fig. 6 (a) indicating their sense of rotation. The lower region is an accumulation of trailing shed vorticity most likely resulting from the tendency of a shear layer to form a vortex which is described by Pullan et al. (2003). In literature this structure is often named the trailing shed vortex but the measurements and the CFD prediction do not show the formation of a distinct vortex at this axial position. The upper peak of the trailing shed vorticity corresponds to the three dimensional separation line which forms on the suction surface in between the passage vortex and the radially migrating suction side boundary layer fluid. This interpretation results from flow visualization which is not shown here due to reasons of brevity. The predicted locations and distributions of the trailing shed vorticity and the passage vortex agrees well with the measured data whilst the intensity is overestimated by the CFD prediction. Nevertheless, the CFD prediction contains an additional flow structure which is marked in Fig. 6 (b). As measured and described by Gregory-Smith et al. (1988) this patch of positive vorticity can be associated with a corner vortex (CV). The data measured does not show any evidence of a corner vortex, this is probably due to inadequate measurement resolution. The hub cavity which starts at the axial location of the traverse plane has no significant influence on the measurement or the prediction. Overall, the CFD prediction provides a good reproduction of the NGV exit flow in terms of wake and secondary flow structures.

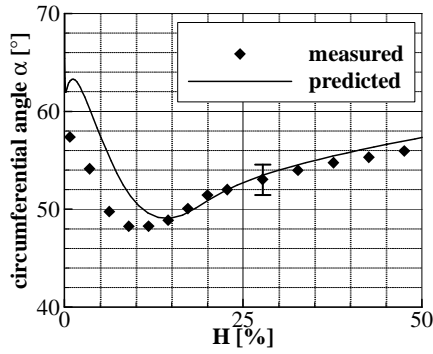


**Fig. 4** Circumferentially mass-averaged absolute circumferential flow angle  $\alpha$  at NGV exit

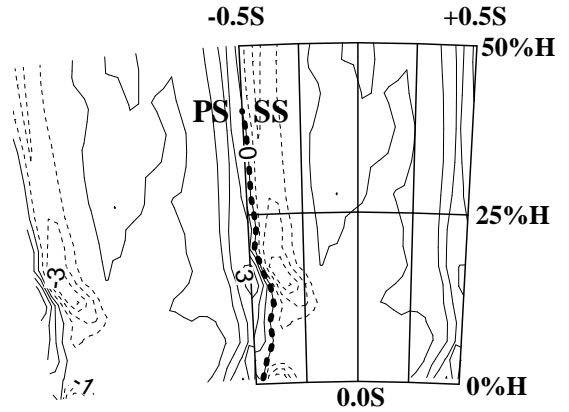


**Fig. 5** Measured radial vorticity  $\omega_r$  at NGV exit in the absolute frame of reference; solid lines:  $\omega_r > 0$ ; dashed lines:  $\omega_r < 0$ ; contour interval  $\Delta\omega_r=1.0$

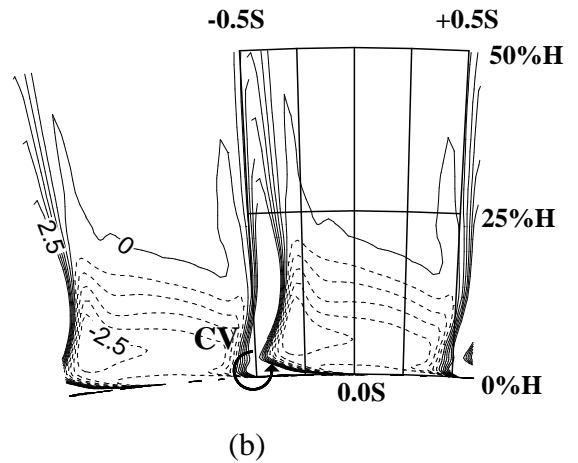
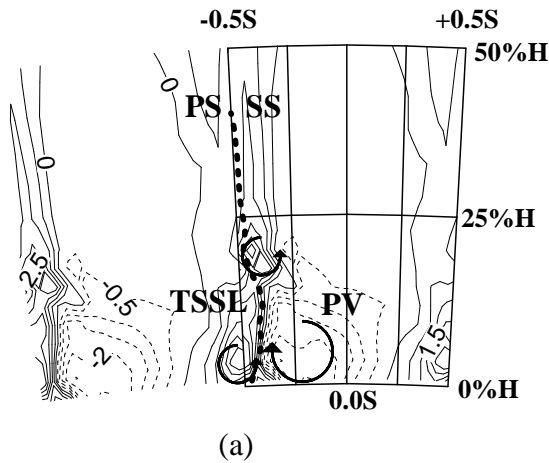


**Fig. 6** Measured (a) and predicted (b) streamwise vorticity  $\omega_s$  at NGV exit in the absolute frame of reference; solid lines:  $\omega_s > 0$ ; dashed lines:  $\omega_s < 0$ ; contour interval  $\Delta\omega_s=0.5$

### Vane-Rotor Interactions

The NGV wake and vortical structures both interact with the rotor blade in a four-dimensional process. The analysis must take the three dimensions of space as well as the time dimension into account. The URANS prediction provides a highly resolved data set in space and time inside the rotor passage for this approach. One transit of the NGV flow structures through the hub rotor passage is shown by four distinct time-steps in the relative frame of reference in Fig. 7 (a) to (d). The time-steps are given in non-dimensional blade passing time  $t/T$ . The angles of view differ for each of the images to improve the insight into the four-dimensional flow field. The iso-surfaces represent fixed levels of streamwise vorticity. They are held constant throughout the image series. The trailing shed vorticity and the passage vortex can be distinguished by the sign of the streamwise vorticity (bright (+) and dark (-) regions, respectively). To give an orientation in space, the leading and the trailing edges (LE and TE), the suction and the pressure sides (SS and PS), as well as the endwall and the line of 25 % channel height are highlighted. Skewed boundary layers contain substantial levels of streamwise vorticity. Therefore the iso-surfaces above the suction and the pressure side are blanked generally to improve clarity.

The Fig. 7 (a) presents the time step  $t/T=0.1875$  in which the NGV trailing shed vorticity and the passage vortex enter the rotor passage at the hub. The view is from upstream into the rotor passage. The data is sliced at 50 % axial gap between NGV trailing edge and rotor leading edge. For

comparison this axial position represents the traverse plane shown in Fig. 6. Please note that the level of streamwise vorticity has changed compared to the plot at NGV exit for two reasons. First the mass-averaged absolute velocity at rotor exit has been chosen to non-dimensionalize the streamwise vorticity within the rotor passage to be consistent with the rotor exit measurements shown later. Secondly the frame of reference has changed. The absolute velocity at rotor exit is smaller by about a factor of 1.5 compared to the velocity at NGV exit resulting in higher values of streamwise vorticity.

In Fig. 7 (a) is shown that the NGV flow structures enter the rotor passage with marginal deformations until they impinge on the pressure side and then, subsequently, get sliced by the leading edge of the adjacent rotor blade. The process of vortex cutting by a turbine blade has been described in detail by Binder (1985) and experimentally captured by Aurahs et al. (2009). URANS is not capable of resolving the details of vortex cutting; e.g. vortex breakdown. Still, the remarkably good agreement between the prediction and the measurement at rotor exit provides the confidence that URANS resolves the general underlying physics of secondary flow interaction. The validation at rotor exit is presented in the next chapter. The time step  $t/T=0.75$  which is plotted in Fig. 7 (b) reveals a strong interaction process of the rotor leading edge region and the NGV trailing shed shear layer (TSSL) as well as the NGV passage vortex (PV). The view is through an adjacent rotor blade into the passage and onto the suction side of the rotor blade. The flow direction is from the left to the right hand side. A process similar to the convection of a wake segment within a blade row as reported by e.g. Stieger and Hodson (2005) is observed for the secondary flow structures. The authors characterize the different processes of wake convection with bowing, reorientation, elongation, and stretching.

In Fig. 7 (b) the equivalent process of bowing for low momentum secondary flow fluid is shown which is generated by the higher midpassage velocities compared to the velocities near the blade surfaces. The lower part of the trailing shed shear layer is less bowed to the suction side of the blade compared to the upper part due to the blockage effect of the passage vortex. Subsequently the upper part of the trailing shed shear layer experiences regions of high velocities at the suction side of the blade whilst the lower part of the trailing shed vorticity travels along the pressure side in regions of low velocities. Consequently a shearing process develops which splits the trailing shed shear layer into two distinct regions of streamwise vorticity labelled with  $TSSL_{up}$  (upper) and  $TSSL_{low}$  (lower). Free shear layers exhibit instability and tend to roll up into a vortex. This has been studied by Pullan et al. (2003). They report the roll up of the NGV trailing shed shear layer into a distinct vortex before entering the rotor. The transformation of the upper trailing shed shear layer into a “sausage-like” flow structure is shown in Fig. 7 (c) and (d) for the time steps  $t/T=1.1875$  and  $t/T=1.5625$ . The view is onto the late suction side of the rotor. The dashed lines represent the rotor trailing edge (TE). The slice at exit is perpendicular to the axial direction. The transformation is interpreted as a roll up into a vortex similar to the one reported by Pullan et al. (2003) but inside the rotor passage and unsteady. Fig. 7 (d) shows the lower part of the trailing shed shear layer undergoing a similar process which can be distinguished from the formation of the rotor passage vortex (rPV). The rotor passage vortex is identified as the thin layer of positive streamwise vorticity on the endwall in between two NGV wakes. The streamwise vorticity of the rotor passage vortex has the same sign as the trailing shed vorticity. Therefore a merging process of the rotor passage vortex and the NGV trailing shed shear layer cannot be excluded. But, regarding the evolution of the lower part of the trailing shed shear layer and the proximity of adjacent NGV wake and secondary flow structures the results indicate that the rotor passage vortex plays a minor role in the formation of the hub rotor secondary flow of this turbine stage.

The rotor secondary flow is observed to be strongly altered by the incoming NGV wakes and secondary flow structures. It differs considerably compared to the classical secondary flow of a cascade; for comparison it is referred to Fig. 1. However, the NGV upstream has a more classical flow structure and has no significant inlet streamwise vorticity. Consequently cascade

measurements have to be treated with care regarding the level of realism of the secondary flow structures. This observation is in line with the results reported by Denton and Pullan (2012). Furthermore, today many companies are designing turbines with endwall profiling to suppress secondary loss; see e.g. Germain et al. (2010). Generally the endwall optimization is performed using steady CFD which is not capable of resolving secondary flow interactions due to the mixing plane approach. Here we can see that the rotor secondary flow is dominated by the NGV streamwise vorticity. It can be concluded that URANS CFD should improve endwall and near-wall blade profile optimization of rotors considerably by resolving the dominating interaction processes. However, this is not yet a practical approach due to computational expense.

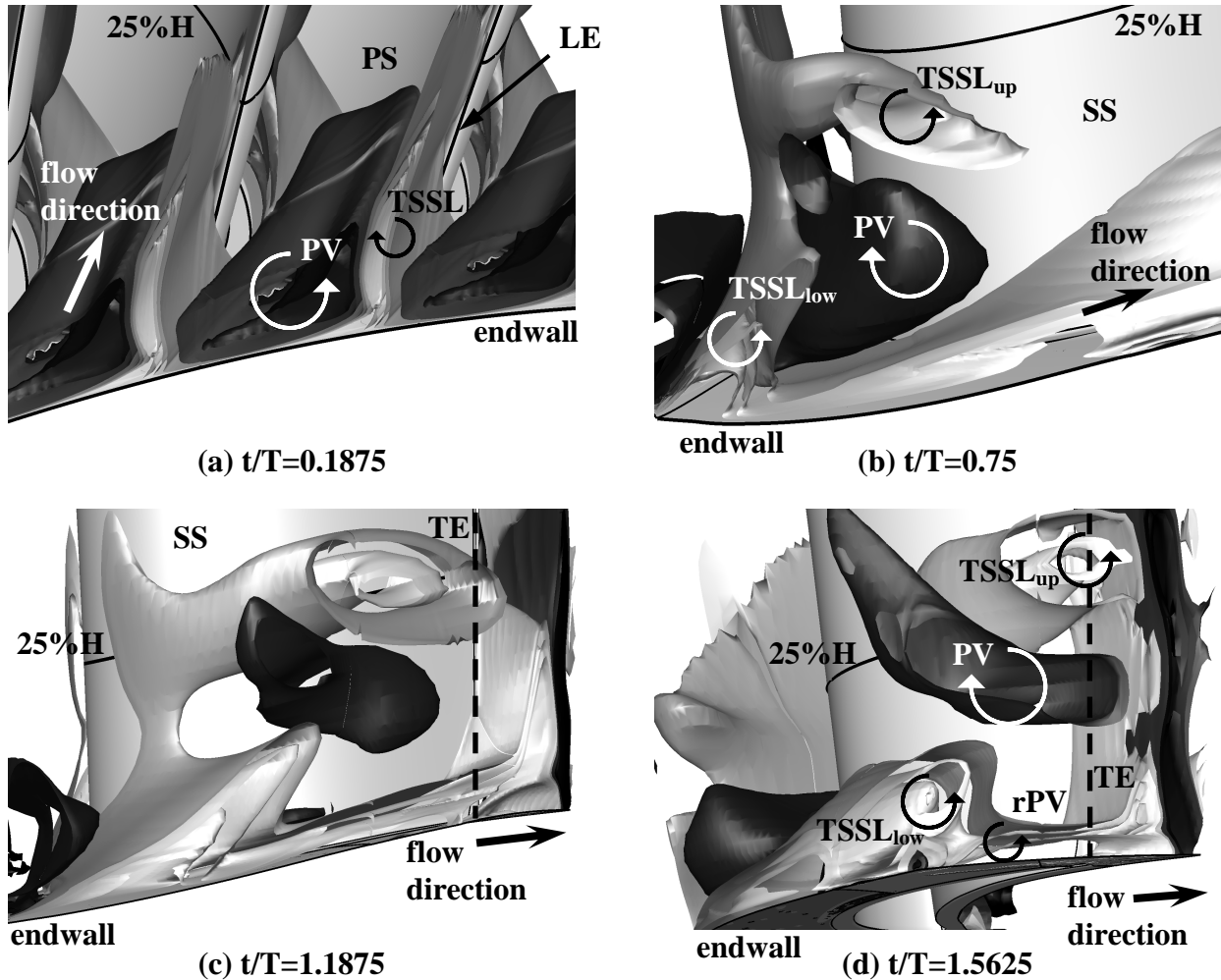


**Fig. 7 Iso-surfaces of streamwise vorticity inside the rotor passage in the relative frame of reference with iso-surface levels of -6, -4, -2, 2, 4, and 6**

### Secondary Flow Structures at Rotor Exit

The vane-rotor interaction features form distinct flow structures at rotor exit. The time-averaged flow field in the absolute frame of reference is analyzed since it determines the steady inlet conditions for the NGV of the downstream stage. A comparison of the predicted and the measured circumferentially mass-average absolute circumferential flow angle  $\alpha$  at stage exit is provided in Fig. 8 including the absolute uncertainty via an error bar. The averaged values as well as the main gradients are well predicted.

The NGV wakes and the secondary vortices are cut to segments by the rotor and travel along wake avenues in the absolute frame of reference as reported by Binder et al. (1989). Therefore the NGV wake and secondary flow structures manifest at fixed circumferential positions at rotor exit, whilst the rotor flow structures average out to circumferentially distributed structures. The time-

averaged NGV wake avenues at rotor exit are presented in Fig. 9 using the measured radial vorticity  $\omega_r$ . The approximate center of the NGV wake avenue is marked by the dashed line ( $\omega_r=0$ ). The negative radial vorticity associated with the suction side part of the NGV wake is hardly noticeable. The diffusive character of the wake is attributed to the mixing processes occurred on the wake's path through the rotor as well as the wake reorientation described by Stieger and Hodson (2005).

The secondary flow field at rotor exit in the absolute frame of reference is presented using the streamwise vorticity  $\omega_s$  shown in Fig. 10 (a) and (b). The black grid marks one pitch and is fixed relative to the NGV trailing edge to be able to compare circumferential positions measured and predicted. The URANS prediction shows good agreement with the measurement at rotor exit. The agreement is fundamentally important to allow for the application of URANS CFD to analyze the rotor passage flow field. The time-averaged results of the vane-rotor interaction phenomena described can be well recognized in the measured and in the predicted streamwise vorticity. The counter clockwise rotating structure  $TSSL_{low}$  is associated with the roll up of the lower part of the NGV trailing shed shear layer, the clockwise rotating structure PV is connected to the NGV passage vortex, and the counter clockwise rotating structure  $TSSL_{up}$  is the result of the roll up of the upper part of the NGV trailing shed shear layer.

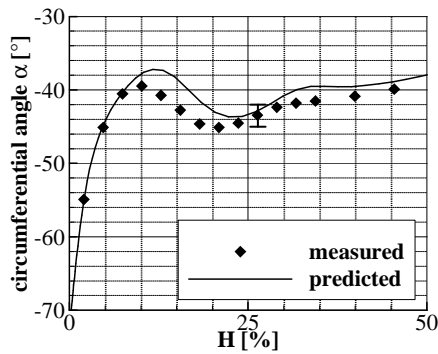


**Fig. 8 Circumferentially mass-averaged absolute circumferential flow angle  $\alpha$  at rotor exit**

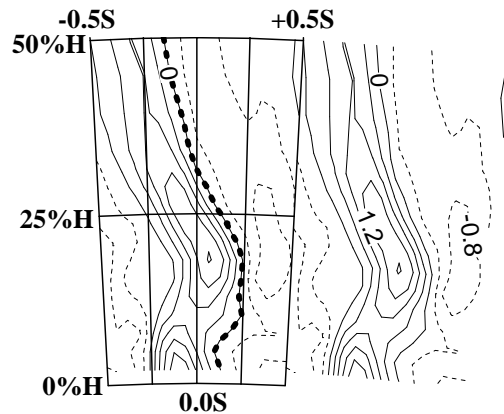
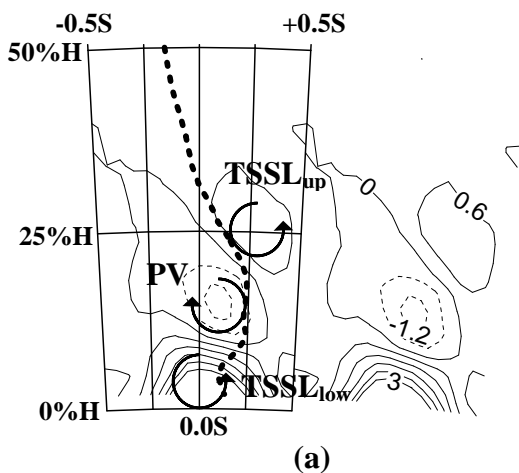
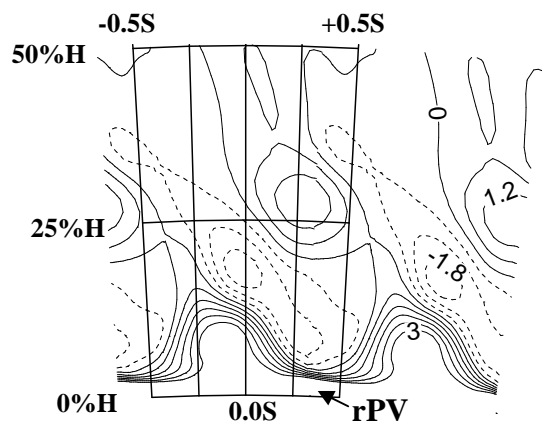


**Fig. 9 Measured radial vorticity  $\omega_r$  at rotor exit in the absolute frame of reference; solid lines:  $\omega_r > 0$ ; dashed lines:  $\omega_r < 0$ ; contour interval  $\Delta\omega_r=0.4$**



(a)



(b)

**Fig. 10 Measured (a) and predicted (b) streamwise vorticity  $\omega_s$  at rotor exit in the absolute frame of reference; solid lines:  $\omega_s > 0$ ; dashed lines:  $\omega_s < 0$ ; contour interval  $\Delta\omega_s=0.6$**

The comparison of Fig. 7 (d) with Fig. 10 (a) (or (b)) shows that the radial positions of the structures agree well. The circumferential alignment of the three structures is explained by the wake elongation resulting from the different velocities of the rotor suction side region compared to the pressure side region and the rotational direction of the rotor. The upper part of the trailing shed shear layer leaves the rotor first due to its path in the vicinity of the suction side of the rotor, followed by the passage vortex and the lower part of the trailing shed vorticity. The latter has travelled mainly on the pressure side of the rotor. The rotational direction of the rotor blade is from the right hand side to the left hand side resulting in a circumferentially shifted time-averaged position of the  $TSSL_{low}$  relative to the  $TSSL_{up}$ . The rotor exit flow in the absolute frame of reference is dominated by rotational structures resulting from the NGV wakes and secondary flows up to approximately 30 % channel height. The layer of positive vorticity on the hub endwall up to  $\sim 3$  % channel height which can be identified in the prediction shown in Fig. 10 (b) is related to the unsteadily transformed rotor hub passage vortex. To avoid damage the five-hole probe measurement has not been performed within this proximity to the endwall. Therefore, the rotor passage vortex is not visible in the measurement shown in Fig. 10 (a).

Finally, in order to show the significance of the subject the impact of the NGV structures on the isentropic efficiency at rotor exit is presented. Fig. 11 shows the measured isentropic efficiency in the absolute frame of reference. The positions of the features  $TSSL_{up}$ , PV, and  $TSSL_{low}$  are marked in the efficiency contour plot. The regions of lowest efficiency at rotor exit correspond well with the regions in which the NGV structures are located but the peaks of lowest efficiency are somewhat misaligned with the identified centers of the vortical structures. The reason for the misalignment is the inherent characteristic of secondary flow structures. They do not just produce loss by mixing out but also transport high loss endwall fluid. Remarkably the level of the isentropic efficiency at rotor exit is massively influenced by the NGV flow structures; e.g. the local isentropic efficiency is reduced by about 10 % in the secondary flow zones compared to the free stream zones in between the NGV wake avenues. Having identified the source of the flow structures to be the streamwise vorticity of the NGV a strong assumption can be formulated. The rotor loss can be reduced by redistributing or reducing the streamwise vorticity of the NGV. Endwall profiling has already shown to redistribute streamwise vorticity as reported by e.g. Jenny (2012). That hidden indirect benefit is likely to be one reason for performance improvements due to endwall profiling. Furthermore a reduction of streamwise vorticity can be achieved by redesigning the lift distribution. According to Hawthorne (1955) that alters the trailing shed vorticity of the airfoil directly.

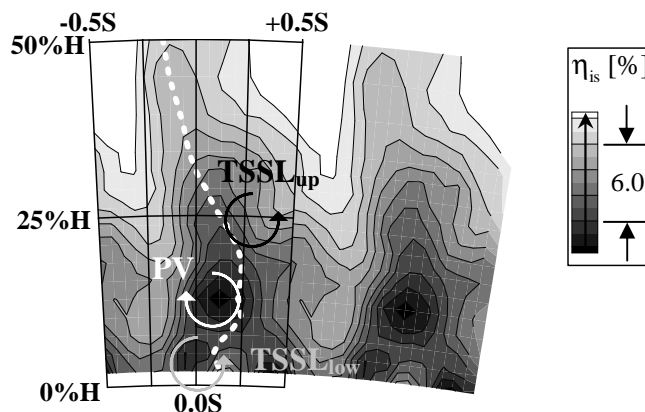


**Fig. 11 Measured isentropic efficiency  $\eta_{is}$  at rotor exit in the absolute frame of reference**

## CONCLUSIONS

A URANS CFD prediction validated by five-hole probe measurements has been used to analyze the unsteady secondary flow field at the rotor hub of a low pressure turbine stage at a low Reynolds number. The following conclusions are drawn:

- The streamwise vortical structures at NGV exit are responsible for the formation of similar structures at rotor exit in the absolute frame of reference.
- Inside the rotor passage the NGV passage vortex and the NGV trailing shed shear layer interact with each other and with the rotor blade.
- This interaction causes the splitting of the NGV trailing shed shear layer in two parts and their subsequent roll ups as a pair of vortices at different heights.
- The secondary flow within a real turbine differs considerably to the secondary flow in cascades due to these unsteady interaction phenomena.
- The optimization of rotor endwalls and near-wall blade profiles should be improved considerably by the application of multi-stage URANS CFD by resolving the dominating flow interactions. Unfortunately, regarding the computational effort this is impractical so far.
- The NGV secondary flow structures alter the stage efficiency significantly; e.g. at the hub the local isentropic efficiency of the secondary flow zone is reduced by about 10 % compared to the free stream zone in between the NGV wake avenues.
- The analysis indicates that rotor loss can be controlled to a degree by NGV design. The level of NGV trailing shed vorticity can be directly manipulated by changing the lift distribution.
- Today endwall profiling is used to reduce the intensity of streamwise vorticity. Therefore NGV endwall profiling may have the hidden benefit of reducing rotor loss already.

## ACKNOWLEDGEMENTS

The authors are grateful for the opportunity to publish results from the research cooperation between MTU Aero Engines GmbH and the Institute of Aircraft Propulsion Systems of the University of Stuttgart. The authors would like to thank the German government for providing the funding through LuFo IV and the former colleagues N. Schinko and M. Kuerner for having performed the measurements.

## REFERENCES

- Aurahs, L., Kasper, C., Kuerner, M., Rose, M. G., Staudacher, S., Gier, J., (2009): “*Water Flow Model Turbine Flow Visualization Study of the Unsteady Interaction of Secondary Flow Vortices with the Downstream Rotor*”, J. of Power and Energy, Vol. 223 no. 6, pp. 677-686.
- Binder, A. (1985): “*Turbulence Production Due to Secondary Vortex Cutting in a Turbine Rotor*”, Journal of Engineering for Gas Turbines and Power, Vol. 107, pp. 1039-1046.
- Binder, A., Forster, W., Mach, K., Rogge, H., (1987): “*Unsteady Flow Interaction Caused by Stator Secondary Vortices in a Turbine Rotor*”, J TURBOMACH, Vol. 109, pp. 251-257.
- Binder, A., Schroeder, Th., Hourmouziadis, J., (1989): “*Turbulence Measurements in a Multistage Low-Pressure Turbine*”, J TURBOMACH, Vol. 111, pp. 153-161.
- Denton, J., Pullan, G., (2012): “*A Numerical Investigation into the Sources of Endwall Loss in Axial Flow Turbines*”, ASME Conf. Proc., GT2012-69173.
- Germain, T., Nagel, M., Raab, I., Schüpbach, P., Abhari, R. S., Rose, M., (2010): “*Improving Efficiency of a High Work Turbine Using Nonaxisymmetric Endwalls – Part I: Endwall Design and Performance*”, J TURBOMACH, Vol. 132.

- Gregory-Smith, D. G., Graves, C. P., Walsh, J. A., (1988): “*Growth of Secondary Losses and Vorticity in an Axial Turbine Cascade*”, J TURBOMACH, Vol. 110, pp. 1-8.
- Hawthorne, W. R., (1955): “*Rotational Flow Through Cascades – Part I. The Components of Vorticity*”, Quart. Journ. Mech. and Applied Math., Vol. VIII.
- Jenny, P., (2012): “*Interaction Mechanisms between Rim Seal Purge Flow and Profiled End Walls in a Low-Pressure Turbine*”, PhD Thesis, ETH Zurich No. 20429.
- Kuerner, M., Schneider, C., Rose, M. G., Staudacher, S., Gier, J., (2010): “*LP Turbine Reynolds Lapse Phenomena: Time-averaged Area Traverse and Multi-stage CFD*”, ASME Conf. Proc., GT2010-23114.
- Kuerner, M., Reichstein, G. A., Schrack, D., Rose, M.G., Staudacher, S., Gier, J., Engel, K., (2011): “*LP Turbine Secondary Vortices: Reynolds Lapse*“, ASME Conf. Proc., GT2011-45557.
- Langston, L. S., (2001): “*Secondary Flows in Axial Turbines – A Review*”, Heat Transfer in Gas Turbine Systems, Annals of the New York Academy of Sciences, 934(1), pp. 11-26
- Niehuis, R., Lücking, P., Stubert, B., (1990): “*Experimental and Numerical Study on Basic Phenomena of Secondary Flows in Turbines*”, AGARD Conf. Proc. No. 469, pp. 5.1-5.17
- Nitsche, W., Brunn, A., (2006): “*Strömungsmesstechnik*“, ISBN–10 3-540-20990-5.
- Pullan, G., Denton, J., Dunkley, M., (2003): “*An Experimental and Computational Study of the Formation of a Streamwise Shed Vortex in a Turbine Stage*”, J TURBOMACH, Vol. 125, pp. 291-297.
- Pullan, G., (2006): “*Secondary Flow and Loss Caused by Blade Row Interaction in a Turbine Stage*”, J TURBOMACH, Vol. 128, pp. 484-491.
- Roeber, T., Kozulovic, D., Kügeler, E., Nürnberger, D., (2006): “*Appropriate Turbulence Modelling for Turbomachinery Flows Using a Two-Equation Turbulence Model*”, New Results in Numerical and Experimental Fluid Mechanics V, Vol. 92, pp. 446-454
- Schinko, N., (2012): “*Verfahren zur Optimierung von zweidimensionalen Strömungsberechnungen während der Turbinenerprobung*“, PhD Thesis, Institute of Aircraft Propulsion Systems, University of Stuttgart.
- Sharma, O. P., Butler, T. L., (1987): “*Predictions of Endwall Losses and Secondary Flows in Axial Flow Turbine Cascades*”, J TURBOMACH, Vol. 109, pp. 229-236.
- Sieverding, C. H., (1985): “*Recent Progress in the Understanding of Basic Aspects of Secondary Flows in Turbine Blade Passages*”, Journal of Engineering for Gas Turbines and Power, Vol. 107, pp. 248-257.
- Stieger, R. D., Hodson, H. P. (2005): “*The Unsteady Development of a Turbulent Wake Through a Downstream Low-Pressure Turbine Blade Passage*“, J TURBOMACH, Vol. 127, pp. 388-394.